IMMUNOTHERAPY

Enhanced CAR-T cell activity against solid tumors by vaccine boosting through the chimeric receptor

Leyuan Ma[1,2], Tanmay Dichwalkar[1], Jason Y. H. Chang[1], Benjamin Cossette[1], Daniel Garafola[1], Angela Q. Zhang[1], Michael Fichter[1], Chensu Wang[1], Simon Liang[1], Murillo Silva[1], Sudha Kumari[1], Naveen K. Mehta[1,3], Wuhbet Abraham[1], Nikki Thai[1], Na Li[1], K. Dane Wittrup[1,3,4], Darrell J. Irvine[1,2,3,5,6]*

Chimeric antigen receptor–T cell (CAR-T) therapy has been effective in the treatment of hematologic malignancies, but it has shown limited efficacy against solid tumors. Here we demonstrate an approach to enhancing CAR-T function in solid tumors by directly vaccine-boosting donor cells through their chimeric receptor in vivo. We designed amphiphile CAR-T ligands (amph-ligands) that, upon injection, trafficked to lymph nodes and decorated the surfaces of antigen-presenting cells, thereby priming CAR-Ts in the native lymph node microenvironment. Amph-ligand boosting triggered massive CAR-T expansion, increased donor cell polyfunctionality, and enhanced antitumor efficacy in multiple immunocompetent mouse tumor models. We demonstrate two approaches to generalizing this strategy to any chimeric antigen receptor, enabling this simple non–human leukocyte antigen–restricted approach to enhanced CAR-T functionality to be applied to existing CAR-T designs.

Chimeric antigen receptor–T cell (CAR-T) immunotherapy targeting the CD19 antigen has produced some marked clinical responses in patients with leukemia and lymphoma, including a high proportion of durable complete remissions (*1*, *2*). However, poor functional persistence of CAR-Ts in some patients results in disease progression (*3*). Despite the success of CAR-T therapy in hematological cancers, it has to date been much less effective for solid tumors, and strategies to enhance efficacy in this setting remain an important goal (*4*, *5*). Therapeutic vaccination is one well-established approach to enhance endogenous T cell responses against cancer (*6*). Several groups have demonstrated the concept of preparing CAR-Ts from virus-specific endogenous lymphocytes or introducing a CAR together with a second antigen receptor specific for a target peptide and then vaccinating recipients against the viral or secondary antigen to boost CAR-T therapy (*7*–*9*). However, these approaches suffer from being human leukocyte antigen (HLA) restricted, and the use of endogenous T cell receptors (TCRs) may be superseded by recent advances where CARs genetically targeted to the native TCR locus (thereby deleting the native TCR) have significantly enhanced activity (*10*).

We recently developed a strategy to target vaccines to lymph nodes by linking peptide antigens to albumin-binding phospholipid polymers (*11*). Small peptides are normally rapidly dispersed into the blood after parenteral injection, but binding of amphiphile peptides to endogenous albumin, which constitutively traffics from blood to lymph, retargets these molecules to lymph nodes (LNs). In addition to exhibiting efficient lymph trafficking, these lipid-tailed molecules can also insert into cell membranes (*12*). We therefore hypothesized that by attaching a small molecule, peptide, or protein ligand for a CAR to the same polymer-lipid tail, CAR ligands could be delivered by albumin to LNs and subsequently partition into membranes of resident antigen-presenting cells (APCs), thereby codisplaying the amphiphile ligand (amph-ligand) from the APC surface together with native cytokine-receptor costimulation (Fig. 1A). Here we show how the dual properties of amph-ligands, lymph node targeting and membrane insertion, combine to create a booster vaccine for CAR-Ts. This amph-ligand strategy safely expands CAR-Ts in vivo, while increasing their functionality and enhancing antitumor activity in multiple models of solid tumors.

To test the ability of amph-ligands to functionally decorate APCs in vivo, we first employed a recently described "retargetable" CAR recognizing the small molecule fluorescein isothiocyanate (FITC), which is directed against tumors by coadministration of a FITC-conjugated antitumor antibody (*13*). The anti-FITC scFv 4m5.3 peptide (*14*) was fused to the CD8α transmembrane domain followed by CD28 and CD3ζ intracellular domains; the cognate amph-ligand for this murine CAR is FITC-poly(ethylene glycol) (PEG)–1,2-distearoyl-*sn*-glycero-3-phosphoethanolamine (amph-FITC; Fig. 1B). When incubated with model APCs in vitro, amph-FITC was absorbed into the plasma membrane in a dose-dependent manner, and despite ongoing endocytosis, many molecules remained accessible to surface staining with an anti-FITC antibody (Fig. 1, C and D). Amph-FITC–coated cells stimulated FITC–CAR-Ts in a dose-dependent manner and were killed by FITC–CAR-Ts (Fig. 1, E and F).

On the basis of these findings, we next tested whether amph-FITC molecules could decorate APCs in LNs to prime FITC-CAR-Ts in vivo. Subcutaneous (s.c.) immunization of mice with free FITC did not result in accumulation in the draining LNs, whereas 10 nmol of amph-FITC was detectable for 21 days (fig. S1A). Amph-FITC primarily accumulated in draining LNs, with low to negligible levels detectable in the liver, spleen, and other organs (fig. S1B). Confocal imaging of LNs showed that amph-FITC initially accumulated in interfollicular regions but partitioned onto $CD11c^+$ dendritic cells (DCs) in T cell areas over time (Fig. 2, A and B, and fig. S1C). Surface-displayed FITC could be detected on sorted $FITC^+$ $CD11c^+$ cells stained with an antibody against FITC (Fig. 2C and fig. S1D). In contrast to the efficient amph-FITC insertion into the membranes of many LN cell types in vitro, surface-accessible FITC was present primarily on macrophages and $CD11c^+$ $CD11b^+$ DCs in vivo (Fig. 2D and fig. S2, A and C). DCs line collagen conduits that carry lymph fluid into the LN, and we hypothesize that the anatomic structure of LNs in part dictates preferential access of these cells to amph-vax molecules entering LNs (*15*). This is supported by the observation that amph-FITC coinjected with a low-molecular-weight dextran [which is known to be transported through the LN conduit system (*16*)] showed substantial colocalization in fiber-like structures extending from the sinuses (fig. S2D). Immunization using amph-FITC together with the STING agonist adjuvant cyclic-di-GMP increased the duration of amph-FITC display on multiple APCs and, as expected, led to up-regulation of costimulatory molecules on amph-$FITC^+$ DCs (Fig. 2E and fig. S2E). Notably, however, surface-accessible FITC decayed quickly and persisted on only a small fraction of cells.

To test the ability of amph-ligand immunization to expand CAR-Ts in vivo, we transferred $CD45.1^+$ FITC-CAR-Ts into lymphocyte (lympho)-depleted congenic $CD45.2^+$ recipient mice and subsequently vaccinated twice with amph-FITC and adjuvant. The CAR-Ts expanded substantially after amph-FITC vaccination, and expansion was increased by coadministering adjuvant (Fig. 2F). For example, transfer of 5×10^4 FITC-CAR-T followed by amph-FITC vaccination with adjuvant expanded these cells to a peak of ~70% of the total $CD8^+$ T cell compartment, yielding a CAR-T population nearly double the size achieved by administering a 200-fold-greater

[1]David H. Koch Institute for Integrative Cancer Research, Massachusetts Institute of Technology, Cambridge, MA 02139, USA. [2]Howard Hughes Medical Institute, Chevy Chase, MD 20815, USA. [3]Department of Biological Engineering, Massachusetts Institute of Technology, Cambridge, MA 02139, USA. [4]Department of Chemical Engineering, Massachusetts Institute of Technology, Cambridge, MA 02139, USA. [5]Department of Materials Science and Engineering, Massachusetts Institute of Technology, Cambridge, MA 02139, USA. [6]Ragon Institute of Massachusetts General Hospital, Massachusetts Institute of Technology, Cambridge, MA 02139, USA.
***Corresponding author. Email: djirvine@mit.edu**

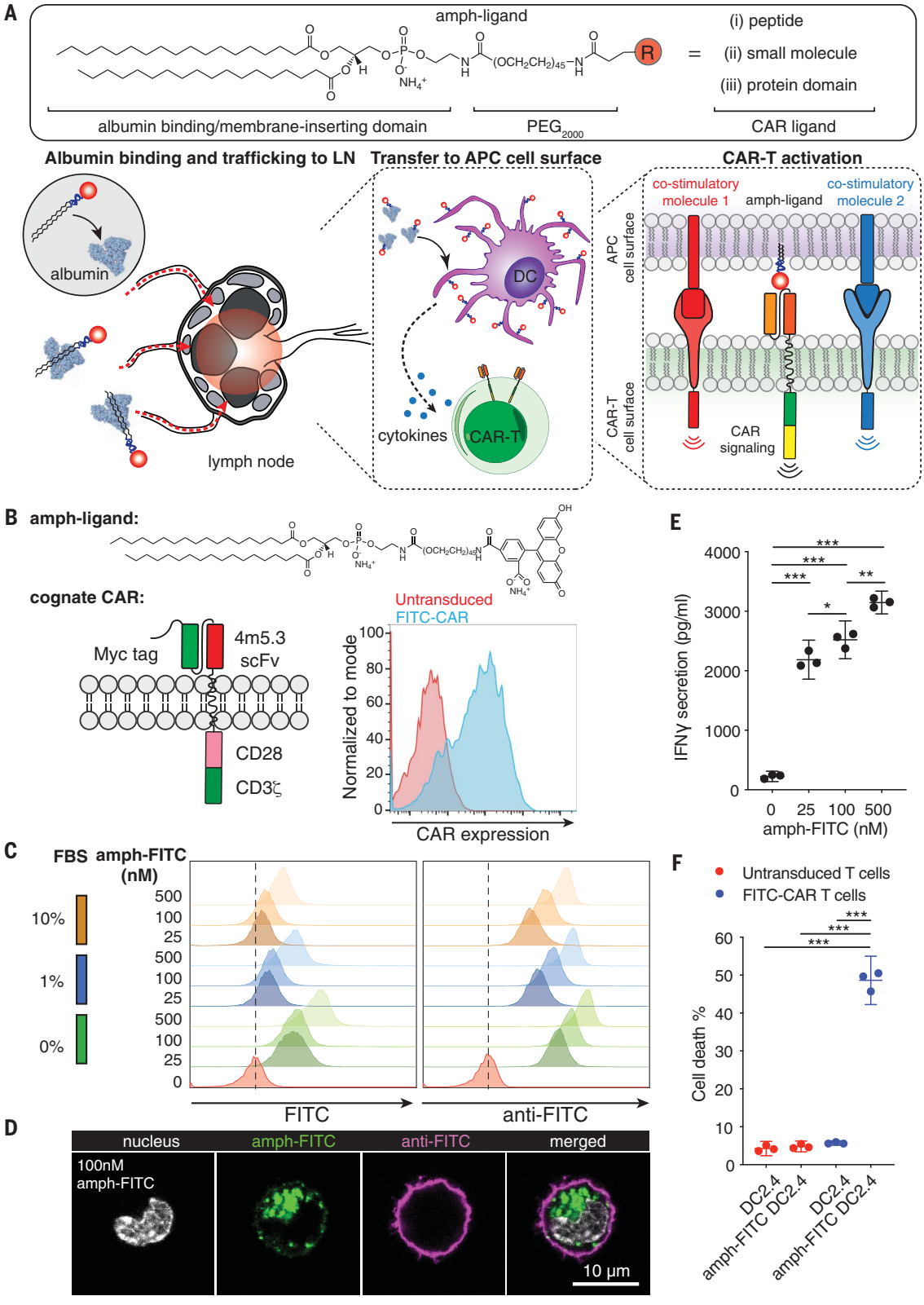

Fig. 1. Design of an amph-ligand vaccine to boost CAR-Ts. (**A**) Schematic of the general chemical structure of amph-ligands (top) and the steps in amph-ligand vaccine boosting in vivo (bottom). Upon injection, amph-ligands associate with albumin at the injection site and are subsequently trafficked to the draining LNs. The amphiphiles then transfer to the membrane of lymph node–resident cells, including APCs. CAR-Ts that encounter decorated APCs in the LNs are stimulated by the surface-displayed amph-ligand as well as costimulatory receptors and cytokines produced by the APCs. (**B**) Structures of amph-FITC and cognate FITC-CAR and a representative flow cytometry analysis of T cell surface expression for FITC-CAR. (**C** and **D**) Flow cytometry analysis at 24 hours (C) and confocal imaging after 30 min (D) of amph-FITC insertion into DC2.4 cell membranes, by direct FITC fluorescence or staining with an anti-FITC antibody. (**E** and **F**) IFN-γ secretion (in picograms per milliliter) (E) and killing (the percentage of target cell death) (F) of amph-FITC–coated DC2.4 cells after 6 hours coculture with FITC–CAR-T or control untransduced T cells at a 10:1 effector:target (E:T) ratio. Shown in (E) and (F) are representative experiments with technical triplicates. *P* values were determined by unpaired Student's *t* test. Error bars represent 95% confidence intervals (CI). ***$P < 0.0001$; **$P < 0.01$; *$P < 0.05$.

number of CAR-Ts without vaccination (Fig. 2F). By 3 weeks after boost, the persisting CAR-Ts were a mixture of effector/effector memory and central memory cells (Fig. 2G). Amph-vax boosting also expanded CAR-Ts in lympho-replete mice; in this setting, two immunizations could expand 10^6 transferred cells from undetectable levels to ~20% of the total CD8 compartment (Fig. 2H). To determine whether professional APCs played an important role in CAR-T priming by amph-ligand immunization, we depleted different cell types in LNs. CAR-T expansion in response to amph-FITC immunization was not impaired in *Batf3*$^{-/-}$ mice lacking cross-presenting DCs, but depletion of total DCs in CD11c-diphtheria

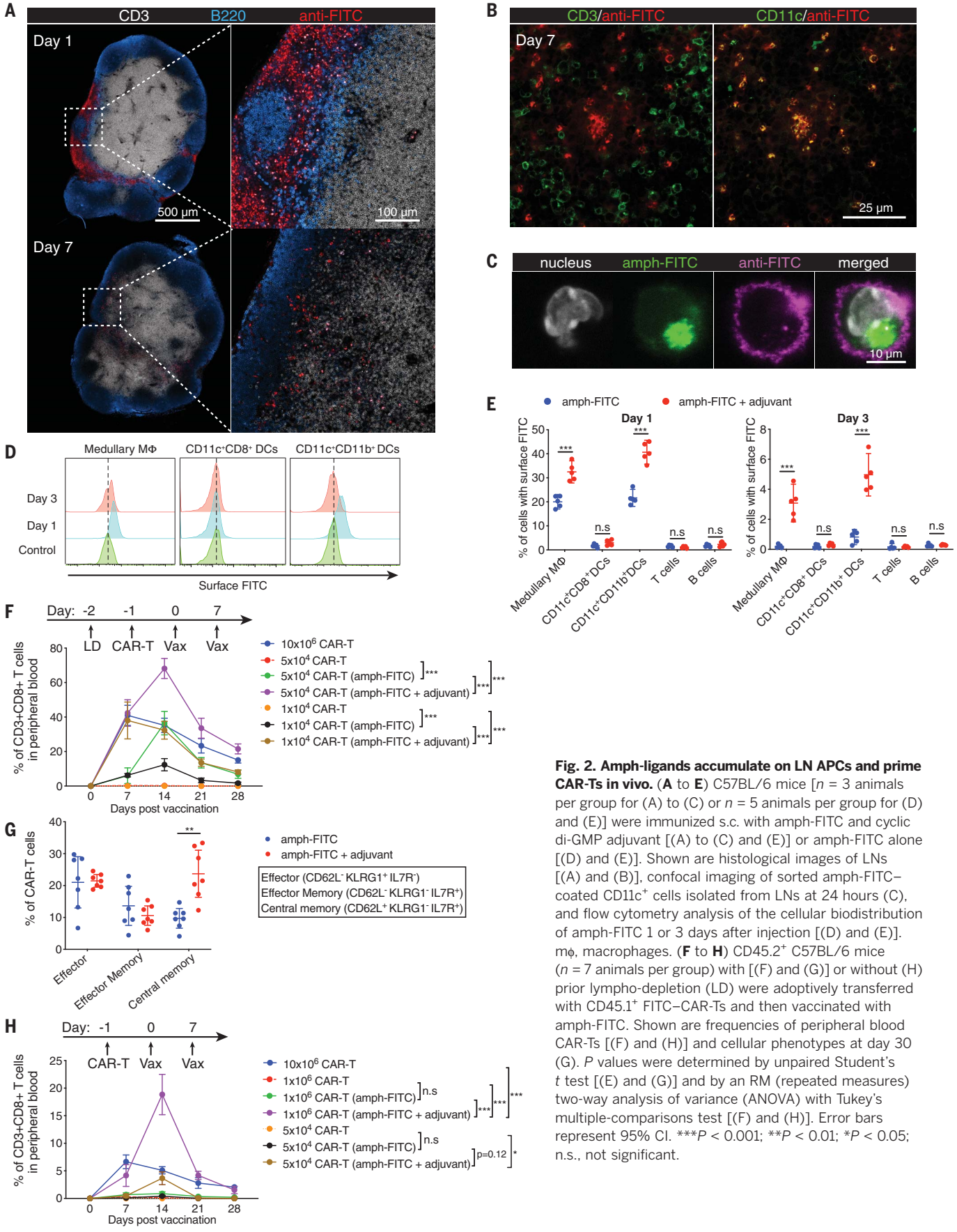

Fig. 2. Amph-ligands accumulate on LN APCs and prime CAR-Ts in vivo. (**A** to **E**) C57BL/6 mice [n = 3 animals per group for (A) to (C) or n = 5 animals per group for (D) and (E)] were immunized s.c. with amph-FITC and cyclic di-GMP adjuvant [(A) to (C) and (E)] or amph-FITC alone [(D) and (E)]. Shown are histological images of LNs [(A) and (B)], confocal imaging of sorted amph-FITC–coated CD11c$^+$ cells isolated from LNs at 24 hours (C), and flow cytometry analysis of the cellular biodistribution of amph-FITC 1 or 3 days after injection [(D) and (E)]. mϕ, macrophages. (**F** to **H**) CD45.2$^+$ C57BL/6 mice (n = 7 animals per group) with [(F) and (G)] or without (H) prior lympho-depletion (LD) were adoptively transferred with CD45.1$^+$ FITC–CAR-Ts and then vaccinated with amph-FITC. Shown are frequencies of peripheral blood CAR-Ts [(F) and (H)] and cellular phenotypes at day 30 (G). P values were determined by unpaired Student's t test [(E) and (G)] and by an RM (repeated measures) two-way analysis of variance (ANOVA) with Tukey's multiple-comparisons test [(F) and (H)]. Error bars represent 95% CI. ***P < 0.001; **P < 0.01; *P < 0.05; n.s., not significant.

toxin receptor (DTR) mice or macrophages using chlodronate liposomes led to significant reductions in CAR–T cell numbers (fig. S3, A to C). In addition, the cytokine functionality of responding CAR-Ts was reduced in all three settings (fig. S3, A to C). In vivo blockade of a collection of costimulatory molecules expressed by APCs also markedly suppressed both FITC–CAR-T expansion and cytokine functionality in response to amph-FITC immunization (fig. S3D).

A key concern with amph-ligand delivery is the potential for toxicity from CAR-T–mediated killing of decorated cells in LNs or other tissues. Consistent with the low fraction of any cell type with detectable surface FITC ligand, no significant changes in viable LN cell populations were detectable 1 day, 3 days, or 14 days after amph-FITC immunization (fig. S4, A to C). No changes in systemic liver enzymes, liver histopathology or CAR-T infiltration, or serum cytokine levels were observed after amph-FITC boosting (fig. S4, D to I). We further evaluated the functional integrity of vaccinated LNs by administering an amph-FITC boost in the presence or absence of transferred FITC-CAR-Ts and then immunizing animals with ovalbumin at the same site 5, 7, or 14 days later (fig. S4J). We observed decreased expansion and functionality of endogenous SIINFEKL-specific T cells when animals were immunized 5 days—but not 7 or 14 days—after amph-FITC boost, suggesting that the combination of CAR-T transfer and amph-FITC vaccination has a short-term effect on priming of endogenous T cell responses [which recovers rapidly (fig. S4K)]. Owing to the lack of T cell help, repeated amph-FITC immunization with adjuvant elicited no antibody response against the amph-ligand itself (fig. S5).

We next evaluated if amph-ligands could be used to prime a bona fide tumor antigen–specific CAR. The EGFRvIII-specific 139scFv CAR recognizes a short linear epitope derived from EGFRvIII (*17*). We prepared murine T cells expressing this CAR and synthesized an amph-vax molecule composed of PEG-DSPE linked to the peptide ligand with or without an N-terminal FITC label (amph-pepvIII; Fig. 3A). Similar to amph-FITC, amph-pepvIII inserted in cell membranes in vitro and the amph-pepvIII–coated cells stimulated EGFRvIII-CAR-Ts (fig. S6, A and B). Immunization of mice with amph-pepvIII triggered EGFRvIII-CAR-T proliferation in vivo (Fig. 3B). To test the therapeutic impact of vaccine boosting, we transduced murine CT-2A glioma cells with EGFRvIII; these cells were efficiently killed by EGFRvIII-CAR-Ts in vitro (fig. S6, C and D). Transfer of EGFRvIII–CAR-T into lympho-depleted CT-2A-mEGFRvIII tumor-bearing mice that were then immunized with amph-pepvIII expanded the CAR-Ts substantially in the periphery (Fig. 3C). Vaccination induced significant increases in the proportion of cells with an effector phenotype (fig. S6E) and 5- to 10-fold increases in CAR–T cell polyfunctionality (Fig. 3D). Amph-vax boosting greatly increased CAR-T infiltration into tumors, and these tumor-infiltrating lymphocytes expressed higher levels of granzyme B and Ki67 than unboosted CAR-Ts (Fig. 3E). In therapeutic studies, animals receiving both CAR-T and repeated amph-vax boosting had significantly delayed tumor growth and prolonged survival (Fig. 3, F and G). Treatment with 1×10^6 CAR-Ts alone led to no long-term survivors, while this same CAR-T dose boosted by amph-vaccination eliminated tumors in a majority of animals (Fig. 3, F and G). Administration of amph-pepvIII with adjuvant in the absence of CAR-Ts had no therapeutic impact (fig. S6F). EGFRvIII–CAR-Ts from vaccinated animals persisted over time, and surviving animals rejected tumor rechallenge at day 75 (fig. S6, G and H). Notably, animals that rejected primary tumors after CAR-T plus amph-vax boosting therapy also rejected rechallenge with parental CT-2A tumor cells lacking the ligand for the CAR-Ts , suggesting induction of an endogenous T cell response against other tumor antigens (fig. S6I). Motivated by this finding, we evaluated the reactivity of splenocytes from CT-2A-mEGFvIII tumor-bearing mice that received CAR-Ts with or without two amph-pepvIII boosts. Enzyme-linked immunosorbent spot (ELISPOT) analysis of interferon-γ (IFN-γ) production by splenocytes cultured with parental CT-2A cells revealed a strong endogenous T cell response against parental tumors (Fig. 3H). Similar to amph-FITC–vaccinated mice, no antibody response was elicited against pepvIII after three rounds of weekly vaccination (fig. S6J). We also evaluated the therapeutic efficacy of CAR-T plus amph vaccination in tumor-bearing mice without lympho-depletion preconditioning. Tumor progression in animals receiving CAR-T alone was indistinguishable from that in animals receiving control untransduced T cells, whereas CAR-T transfer combined with amph-pepvIII immunization delayed tumor growth and prolonged animal survival (Fig. 3, I and J). In both the lympho-depleted and non–lympho-depleted settings, amph-vax boosting was accompanied by small transient alterations in animal body weight and minimal alterations in serum cytokine levels (fig. S6, K and L). To assess the utility of amph-vax boosting with a more potent "third-generation" CAR design, we generated an EGFRvIII-targeting CAR containing both CD28 and 41BB co-stimulatory domains. This CAR was well-expressed and functional in vitro (fig. S7, A and C). We then treated large (~50-mm^2) established CT-2A-mEGFRvIII tumors with EGFRvIII-28BBzCAR-T cells, with or without amph-pepvIII boosting. In this high tumor burden setting, the CAR-Ts alone had a modest impact on tumor progression, and amph-ligand boosting greatly improved tumor control and enhanced overall survival (fig. S7, D and E).

Although use of a peptide ligand for CAR-Ts was effective, some CARs recognize three-dimensional structural epitopes (*18*). As an alternative strategy to amph-ligand boost with any CAR regardless of the nature of its binding domain or specificity, we devised a tandem scFv-based bispecific CAR based on recently reported designs (*19*). The anti-FITC scFv was fused to the N-terminal extracellular domain of a tumor-targeting CAR (TA99) that recognized the melanoma-associated antigen TRP1 (Fig. 4, A and B). FITC/TRP1-CAR-Ts were activated both by amph-FITC-coated target cells and by TRP1-expressing B16F10 cells (fig. S8A), and killed $TRP1^+$ target cells at levels equivalent to those cells expressing monospecific TRP1-CAR (Fig. 4C). In vivo, amph-FITC vaccination stimulated FITC/TRP1-bispecific CAR-T proliferation (fig. S8B). Similar to observations in the EGFRvIII system, amph-vax boosting of FITC/TRP1–CAR-T in B16F10 tumor-bearing animals led to pronounced CAR-T expansion in the periphery and increased tumor infiltration (fig. S8, C and D), with minimal serum cytokine elevation and transient fluctuations in body weight after each vaccination (fig. S8, E and F). Whereas adoptive therapy with FITC/TRP1–CAR-T alone had almost no effect on B16F10 tumor progression, repeated boosting after transfer with amph-FITC led to pronounced slowing in tumor growth and extended survival (Fig. 4, D and E). One resistance mechanism to CAR-T therapy is loss of surface antigen (*20*), but we did not observe apparent Trp1 loss upon tumor outgrowth in this model (fig. S8, G and H). To assess potential autoimmune toxicity induced by amph-vax boosting, we examined thymus and skin tissues (which naturally express Trp1) from treated animals, but we found no changes in histopathology or CAR-T infiltration into the thymus with amph-vax boosting (fig. S8, I to K). We also assessed whether CAR-T therapy with vaccine boosting would be more effective if mixed CD4/CD8 CAR-Ts were used. In vitro, both $CD4^+$ and $CD8^+$ CAR-Ts were activated by culture with amph-ligand–coated target cells (fig. S8L), and similar therapeutic efficacy was observed when B16F10 tumors were treated with CD8 as with mixed CD4/CD8 FITC/Trp1–CAR-Ts boosted by amph-FITC vaccination (fig. S8, M and N).

To assess the broad applicability of this bispecific CAR platform irrespective of animal strain or haplotype and to evaluate treatment of metastatic disease, we prepared 4T1 tumor cells transduced to express mEGFRvIII and luciferase, modeling $EGFRvIII^+$ breast cancer (*21*) on the BALB/c background. A cognate FITC/EGFRvIII-bispecific CAR was generated, which was well-expressed in BALB/c T cells and was functional in vitro and in vivo (fig. S9, A and D). 4T1-mEGFRvIII tumor cells were injected intravenously (i.v.) into BALB/c mice to induce lung metastases and then treated with FITC/EGFRvIII–CAR-T with or without amph-FITC boosting. Tumor progression as assessed by bioluminescence imaging was significantly impacted only when CAR-Ts were supplemented with amph-ligand boosting (fig. S9E), leading to prolonged survival and clearance of tumors in two of five animals (fig. S9F). In the CAR-T plus amph-vax–treated animals that relapsed, EGFRvIII surface levels were markedly reduced, suggesting selection of low-antigen–expressing or null tumor cells during therapy (fig. S9G). Finally, to verify that this bispecific CAR approach could also be used to boost human CAR-T, we constructed a FITC/hCD19-bispecific human

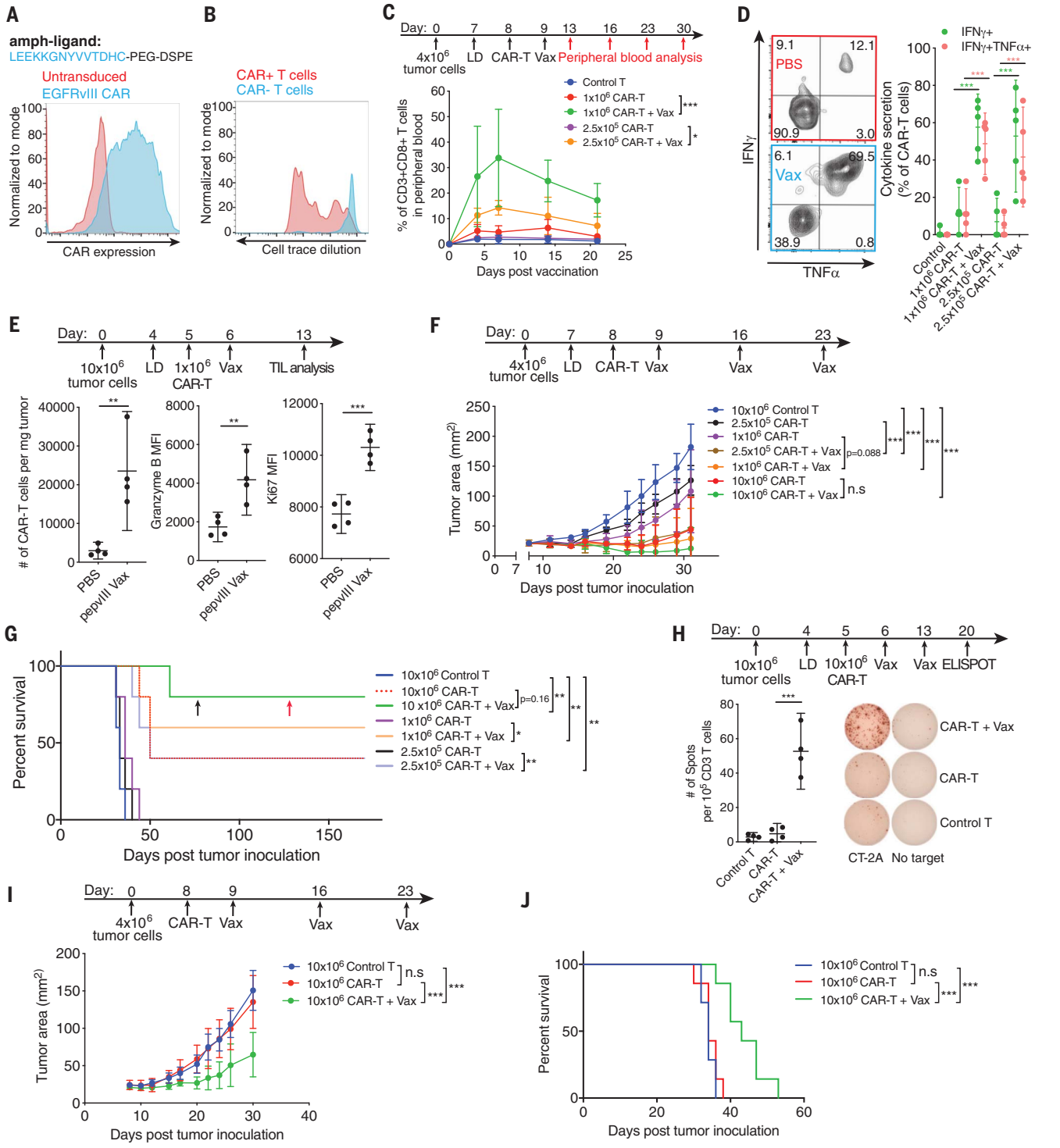

Fig. 3. Amph-peptide ligands boost CAR-Ts in vivo for enhanced solid tumor immunotherapy in mice. (**A**) Structure of amph-pepvIII and surface expression of EGFRvIII CAR. (**B**) Representative histogram showing EGFRvIII–CAR-T proliferation in LNs 48 hours after amph-pepvIII vaccination (n = 3 animals per group). (**C** and **D**) Expansion (C) and cytokine polyfunctionality at day 7 (D) of circulating EGFRvIII–CAR-Ts following a single amph-pepvIII immunization (n = 5 animals per group). (**E**) Enumeration, granzyme B levels, and Ki67 levels of tumor-infiltrating EGFRvIII–CAR-Ts (n = 4 animals per group) with or without amph-pepvIII boost. (**F** to **J**) Tumor growth [(F) and (I)], ELISPOT of enriched $CD3^+$ splenocytes cultured with irradiated parental CT-2A tumor cells (H), and survival [(G) and (J)] of mEGFRvIII-CT-2A tumor-bearing mice treated with EGFRvIII–CAR-T with or without amph-pepvIII vaccination for animals that were lympho-depleted [(F) and (G) n = 5 animals per group; (H) n = 4 animals per group)], or lympho-replete [(I) and (J) n = 7 animals per group)] prior to adoptive transfer. The black arrow indicates time of CT-2A-EGFRvIII tumor rechallenge. The red arrow indicates time of parental CT-2A tumor rechallenge. P values were determined by unpaired Student's t test [(D), (E), and (H)], by an RM two-way ANOVA with Tukey's multiple-comparisons test [(C), (F), and (I)], or by log-rank test [(G) and (J)]. Error bars represent 95% CI. ***P < 0.001; **P < 0.01; *P < 0.05; n.s., not significant.

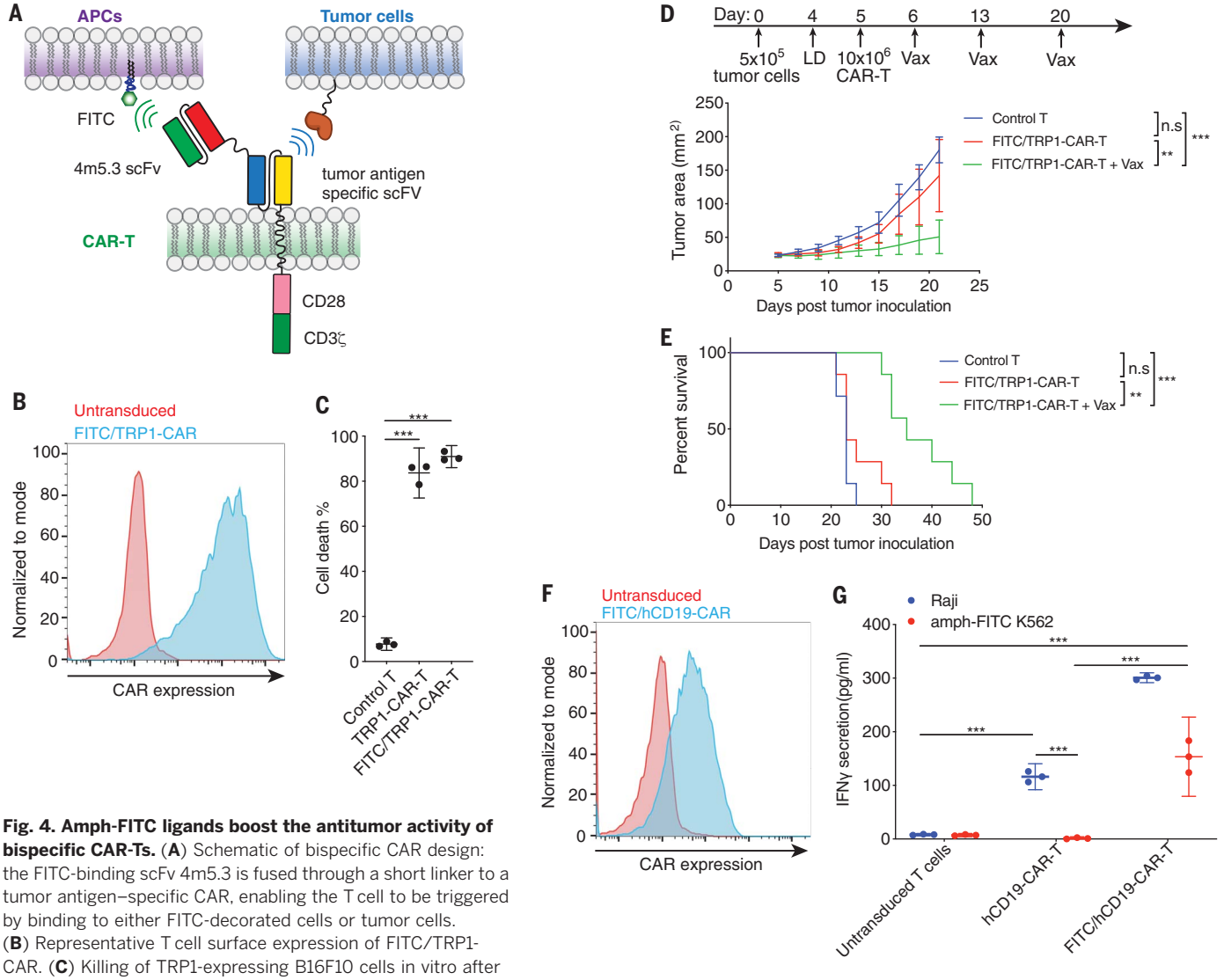

Fig. 4. Amph-FITC ligands boost the antitumor activity of bispecific CAR-Ts. (**A**) Schematic of bispecific CAR design: the FITC-binding scFv 4m5.3 is fused through a short linker to a tumor antigen–specific CAR, enabling the T cell to be triggered by binding to either FITC-decorated cells or tumor cells. (**B**) Representative T cell surface expression of FITC/TRP1-CAR. (**C**) Killing of TRP1-expressing B16F10 cells in vitro after 6-hour coculture with FITC/TRP1–CAR-T, monospecific TRP1–CAR-T, or control untransduced T cells at an E:T of 10:1. (**D** and **E**) Tumor growth (D) and survival (E) of B16F10 tumor-bearing mice (n = 7 animals per group) treated with 10 × 10^6 CAR–Ts alone or CAR-Ts plus amph-FITC vaccination. P values were determined by an RM two-way ANOVA with Tukey's multiple-comparisons test (D) or by log-rank test (E). (**F**) Surface expression of FITC/hCD19-bispecific CAR on human T cells. (**G**) FITC/TRP1-bispecific CAR-Ts responding to either $hCD19^+$ Raji cells or amph-FITC–coated K562 cells as monitored by IFN-γ secretion. Shown in (C) and (G) are representative experiments with technical triplicates. P values were determined by an unpaired Student's t test [(C) and (G)]. Error bars represent 95% CI. ***P < 0.0001; **P < 0.01; *P < 0.05; n.s., not significant.

CAR using the established FMC63 antibody against CD19 (*22*) and expressed this CAR in human T cells (Fig. 4F). Human FITC/hCD19–CAR-Ts were stimulated by both $CD19^+$ Raji cells as well as amph-FITC–coated target cells (Fig. 4G). Altogether, we present here a new vaccine approach to boosting CAR-T numbers and functionality in vivo with low toxicity, enabling enhanced efficacy in syngeneic solid tumor models. Although not directly evaluated here, this approach might be further enhanced by nascent strategies to improve CAR function, such as insertion of the CAR into the *TRAC* locus (*10*). The bispecific vaccinable CAR design with amph-FITC vaccine offers a simple and universal solution to boosting CAR-Ts with any antigen specificity.

REFERENCES AND NOTES

1. A. D. Fesnak, C. H. June, B. L. Levine, *Nat. Rev. Cancer* **16**, 566–581 (2016).
2. D. N. Khalil, E. L. Smith, R. J. Brentjens, J. D. Wolchok, *Nat. Rev. Clin. Oncol.* **13**, 273–290 (2016).
3. S. Guedan *et al.*, *JCI Insight* **3**, e96976 (2018).
4. K. Newick, S. O'Brien, E. Moon, S. M. Albelda, *Annu. Rev. Med.* **68**, 139–152 (2017).
5. C. H. June, R. S. O'Connor, O. U. Kawalekar, S. Ghassemi, M. C. Milone, *Science* **359**, 1361–1365 (2018).
6. S. H. van der Burg, R. Arens, F. Ossendorp, T. van Hall, C. J. Melief, *Nat. Rev. Cancer* **16**, 219–233 (2016).
7. M. Tanaka *et al.*, *Clin. Cancer Res.* **23**, 3499–3509 (2017).
8. X. Wang *et al.*, *Clin. Cancer Res.* **21**, 2993–3002 (2015).
9. C. Y. Slaney *et al.*, *Clin. Cancer Res.* **23**, 2478–2490 (2017).
10. J. Eyquem *et al.*, *Nature* **543**, 113–117 (2017).
11. H. Liu *et al.*, *Nature* **507**, 519–522 (2014).
12. H. Liu, B. Kwong, D. J. Irvine, *Angew. Chem. Int. Ed. Engl.* **50**, 7052–7055 (2011).
13. J. S. Ma *et al.*, *Proc. Natl. Acad. Sci. U.S.A.* **113**, E450–E458 (2016).
14. E. T. Boder, K. S. Midelfort, K. D. Wittrup, *Proc. Natl. Acad. Sci. U.S.A.* **97**, 10701–10705 (2000).
15. M. Sixt *et al.*, *Immunity* **22**, 19–29 (2005).
16. J. E. Gretz, C. C. Norbury, A. O. Anderson, A. E. Proudfoot, S. Shaw, *J. Exp. Med.* **192**, 1425–1440 (2000).
17. J. H. Sampson *et al.*, *Clin. Cancer Res.* **20**, 972–984 (2014).
18. S. N. De Oliveira *et al.*, *J. Transl. Med.* **11**, 23 (2013).
19. E. Zah, M. Y. Lin, A. Silva-Benedict, M. C. Jensen, Y. Y. Chen, *Cancer Immunol. Res.* **4**, 498–508 (2016).
20. E. Sotillo *et al.*, *Cancer Discov.* **5**, 1282–1295 (2015).
21. C. A. Del Vecchio *et al.*, *Cancer Res.* **72**, 2657–2671 (2012).
22. J. N. Kochenderfer *et al.*, *Blood* **116**, 4099–4102 (2010).

ACKNOWLEDGMENTS

We thank the Koch Institute Swanson Biotechnology Center for technical support, specifically, the whole-animal imaging core facility, histology core facility, and flow cytometry core facility. We thank T. Seyfried for providing the CT-2A cell line. **Funding:** This work was supported by the NIH (award EB022433), the Marble Center for Nanomedicine, and Johnson & Johnson. D.J.I. is an investigator of the Howard Hughes Medical Institute. The project

was also supported by award no. T32GM007753 from the National Institute of General Medical Sciences. M.F. was supported by Deutsche Forschungsgemeinschaft grant FI 2249/1-1:1. The content is solely the responsibility of the authors and does not necessarily represent the official views of the National Institute of General Medical Sciences or the National Institutes of Health. **Author contributions**: L.M., D.J.I., and K.D.W. designed the studies. L.M. and D.J.I. analyzed and interpreted the data and wrote the manuscript. L.M, T.D, D.G., A.Q.Z., J.Y.H.C., S.K., B.C, C.W., S.L., M.S., M.F., N.K.M., W.A., N.T., and N.L. performed experiments. **Competing interests:** D.J.I. and L.M. are inventors on international patent application PCT/US2018/051764 submitted by Massachusetts Institute of Technology, which covers the use of amphiphile-vaccine technology as a vaccine for CAR-Ts. D.J.I. is a consultant for Elicio Therapeutics that has licensed IP related to this technology. **Data and materials availability**: Materials are available under a material transfer agreement (contact person D.J.I.).

SUPPLEMENTARY MATERIALS

science.sciencemag.org/content/365/6449/162/suppl/DC1
Materials and Methods
Figs. S1 to S9
References (*23*–*28*)

28 October 2018; accepted 10 June 2019
10.1126/science.aav8692